

Contents lists available at ScienceDirect

# Journal of Crystal Growth

journal homepage: www.elsevier.com/locate/jcrysgro





# Growth and phase transition of Sr<sub>3</sub>Zr<sub>2</sub>O<sub>7</sub> single crystals

Ikuya Fukasawa <sup>a</sup>, Yuki Maruyama <sup>a,\*</sup>, Suguru Yoshida <sup>b</sup>, Koji Fujita <sup>c</sup>, Hidehiro Takahashi <sup>d</sup>, Masataka Ohgaki <sup>d</sup>, Masanori Nagao <sup>a</sup>, Satoshi Watauchi <sup>a</sup>, Venkatraman Gopalan <sup>b,e</sup>, Katsuhisa Tanaka <sup>c</sup>, Isao Tanaka <sup>a</sup>

- <sup>a</sup> Center for Crystal Science and Technology, University of Yamanashi, Miyamae 7-32, Kofu, Yamanashi 400-0021, Japan
- <sup>b</sup> Materials Research Institute, Pennsylvania State University, PA 16802, United States
- <sup>c</sup> Department of Material Chemistry, Graduate School of Engineering, Kyoto University, Katsura Nishikyo-ku, Kyoto 615-8510, Japan
- d Application Development Center, Hitachi High-Tech Science Corporation, Shintomi 2-15-5, Chuo-ku, Tokyo 104-0041, Japan
- <sup>e</sup> Department of Materials Science and Engineering, Pennsylvania State University, PA 16802, United States

### ARTICLE INFO

Communicated by Vincent J. Fratello

Keywords:

A1. Phase diagrams

A2. Growth from melt

A2. Traveling solvent zone growth

A2. Single crystal growth

B1. Oxide

### ABSTRACT

The melting behavior of Ruddlesden-Popper type hybrid improper ferroelectric  $Sr_3Zr_2O_7$  phase in the  $ZrO_2$ –SrO pseudo-binary system was investigated, and its single crystals were successfully grown. A series of the slow-cooling floating zone experiments revealed that  $Sr_3Zr_2O_7$  melts incongruently into  $SrZrO_3$  phase and a liquid and that the compositional range where  $Sr_3Zr_2O_7$  and a liquid coexist is located around 70 mol% SrO composition. Based on the results, we attempted to grow  $Sr_3Zr_2O_7$  single crystals by the traveling solvent floating zone method using SrO-excess solvent and feed. Consequently, many small single crystals of  $Sr_3Zr_2O_7$  phase with several millimeters in size were discovered in the as-grown boules covered with SrO phase. The phase transition behavior of the grown crystals was investigated by differential thermal analysis with polarizing optical microscopy as well as by optical second harmonic generation measurements. We directly observed a reconstruction of orthorhombic twin domains in  $Sr_3Zr_2O_7$  single crystals accompanied by the first-order ferroelectric transition at about  $410\,^{\circ}C$ .

### 1. Introduction

Ferroelectric perovskites have been studied owing to theoretical interest and commercially important applications such as nonvolatile memory, actuators, and sensors [1–3]. In well-known  $ABO_3$  perovskite-type ferroelectrics like BaTiO<sub>3</sub> and PbTiO<sub>3</sub>, polar cation displacements inducing fascinating physical properties including ferroelectricity and piezoelectricity are driven by a so-called second-order Jahn–Teller effect (SOJT) [4]. Electronic structures favoring polar distortions via the SOJT effect are usually achieved by introducing ions with  $nd^0$  or  $ns^2$  electron configuration into the A or B sites. In general, however, the vast majority of  $ABO_3$  perovskites are not ferroelectric because of the absence of such cations, for example,  $Ti^{4+}$ ,  $Nb^{5+}$ ,  $Pb^{2+}$ , and  $Bi^{3+}$ . As a result, a limited number of  $ABO_3$  perovskites are ferroelectrics.

In layered perovskite oxides such as Ruddlesden-Popper (RP) phase

 $A_{n+1}B_n\mathrm{O}_{3n+1}$ , a new mechanism for creating a ferroelectric state through the combination of two or more non-ferroelectric structural distortions has been predicted from recent theoretical work [5–9]. Such a mechanism is symmetry prohibited in simple perovskites, but is allowed in layered derivatives, where rotations and tilts of  $B\mathrm{O}_6$  octahedra serve as the nominally non-polar structural distortions to generate the electric polarization. Since the rotational and tilting distortions are ubiquitous in perovskites, this new ferroelectric mechanism, named hybrid improper ferroelectricity (HIF) [6], offers a large compositional space for the creation of new ferroelectrics. Indeed, a number of layered perovskites have been experimentally shown to be hybrid improper ferroelectrics so far [5,10–13].

In the present work, we focus on an n = 2 RP compound,  $Sr_3Zr_2O_7$ , in which the SrO rocksalt layer is sandwiched between  $(SrZrO_3)_2$  perovskite layers.  $Sr_3Zr_2O_7$  was reported by Yoshida *et al.* [14] as a new hybrid

Abbreviations: SOJT, Second-Order Jahn–Teller effect; RP, Ruddlesden-Popper; HIF, hybrid improper ferroelectricity; TSFZ, traveling solvent floating zone; SCFZ, slow cooling floating zone; FZ, floating zone; DTA, differential thermal analysis; SEM, scanning electron microscopy; EDS, energy-dispersive X-ray spectroscopy; EPMA, electron probe microanalysis; 2D-XRD, 2-dimensional X-ray diffraction analysis; SHG, second harmonic generation.

E-mail address: myuuki@yamanashi.ac.jp (Y. Maruyama).

<sup>\*</sup> Corresponding author.

improper ferroelectric. Moreover, they demonstrated the room-temperature polarization switching and the ferroelectric phase transition around 420 °C. However, the measured polarization (0.3  $\mu C$  cm $^{-2}$ ) was one order of magnitude lower than the calculated polarization (6.75  $\mu C$  cm $^{-2}$ ) [14]. The lower value is due to the polycrystalline nature. In the case of Ca<sub>3</sub>Ti<sub>2</sub>O<sub>7</sub>, another example of RP-type hybrid improper ferroelectrics, the polarization value (6.4  $\mu C$  cm $^{-2}$ ) of single crystals is larger than that of polycrystals (0.6  $\mu C$  cm $^{-2}$ ) [10,12]. For that reason, Sr<sub>3</sub>Zr<sub>2</sub>O<sub>7</sub> single crystals are necessary to clarify the ferroelectric mechanism experimentally and also to stimulate further experimental investigations for discovering many novel classes of ferroelectrics.

Phase diagrams give us valuable information for crystal growth. Although several phase diagrams were reported for the ZrO2-SrO system, information necessary for the crystal growth of Sr<sub>3</sub>Zr<sub>2</sub>O<sub>7</sub> from the melt remains unclear [15–18]. In the phase diagrams reported by Tilloca et al. and Noguchi et al., Sr<sub>3</sub>Zr<sub>2</sub>O<sub>7</sub> phase decomposes into Sr<sub>4</sub>Zr<sub>3</sub>O<sub>10</sub> and SrO phases or Sr<sub>4</sub>Zr<sub>3</sub>O<sub>10</sub> and Sr<sub>2</sub>ZrO<sub>4</sub> phases at an upper stability limit of about 1650 °C [15,16]. This means that melt growth is not available for Sr<sub>3</sub>Zr<sub>2</sub>O<sub>7</sub> because Sr<sub>3</sub>Zr<sub>2</sub>O<sub>7</sub> does not coexist with a liquid phase. On the other hand, Traverse et al. [17] and Yokokawa et al. [18] have reported that Sr<sub>3</sub>Zr<sub>2</sub>O<sub>7</sub> melts incongruently to SrZrO<sub>3</sub> or Sr<sub>4</sub>Zr<sub>3</sub>O<sub>10</sub> phase and a liquid. This melting behavior suggests that Sr<sub>3</sub>Zr<sub>2</sub>O<sub>7</sub> single crystals can be grown by solution growth such as the self-flux, top-seeded solution growth, and traveling solvent floating zone (TSFZ) methods [19,20]. These contradictory results are mainly due to the very high melting point of zirconate compounds. In order to grow Sr<sub>3</sub>Zr<sub>2</sub>O<sub>7</sub> crystals, it is first important to clarify its melting behavior.

In this paper, the slow cooling floating zone (SCFZ) method was utilized to investigate the melting behavior of n = 2 RP  $Sr_3Zr_2O_7$  phase in the ZrO2-SrO system, and the growth of its single crystals was carried out by the TSFZ method based on the results of the SCFZ method. The SCFZ method, a modified version of the floating zone growth technique, is a convenient way to observe the melting behavior of compounds with a high melting point above 1700 °C, including Sr<sub>3</sub>Zr<sub>2</sub>O<sub>7</sub>, without using a crucible. The SCFZ technique has been employed for the investigation of the phase diagram of the MgO-TiO2 system, and also of the phase relation of the  $Li_xLa_{(1-x)/3}NbO_3$  phase [21,22]. Of solution growth techniques, the TSFZ method, an FZ method using a solvent, is a powerful technique requiring no crucible for growing single crystals of incongruent-melting compounds and solid solutions with a high melting point. Here, we optimized the growth conditions such as feed composition, atmosphere, and growth rate, and successfully grew the single crystals of Sr<sub>3</sub>Zr<sub>2</sub>O<sub>7</sub> by the TSFZ method for the first time. Additionally, we obtained single crystals of n = 1 RP  $Sr_2ZrO_4$  by changing the feed composition. The phase transition of the grown Sr<sub>3</sub>Zr<sub>2</sub>O<sub>7</sub> crystals was characterized by differential thermal analysis (DTA) with a polarizing optical microscope and also by temperature-dependent optical second harmonic generation (SHG) measurements.

### 2. Experimental Details

SrCO $_3$  (99.99%) and ZrO $_2$  (99.9%) powders were used as starting materials and mixed in the Sr $_3$ Zr $_2$ O $_7$  stoichiometric composition. The mixture was calcined at 1000 °C for 6 h and then at 1500 °C for 18 h in air using a Pt crucible with a lid. The calcined powder was put into a rubber tube and pressed to form a cylindrical rod under a hydrostatic pressure of 300 MPa. Then the rod was sintered at 1600 °C for 6 h in air. SrO-excess feeds and solvents were prepared by adding SrCO $_3$  powder into a calcinated powder with a desired composition of Sr $_3$ Zr $_2$ O $_7$  and then pressing into a disc or cylindrical shape. They were used for the SCFZ and TSFZ experiments without sintering.

A four-mirror-type infrared-heating furnace (Crystal Systems Corporation, model FZ-T-12000-X-IC-VM-PC-YS) equipped with four 3.0 kW xenon lamps as heat sources was used for the SCFZ and TSFZ experiments. The SCFZ experiments were performed according to the following process. The edges of the sintered rods mounted on the upper

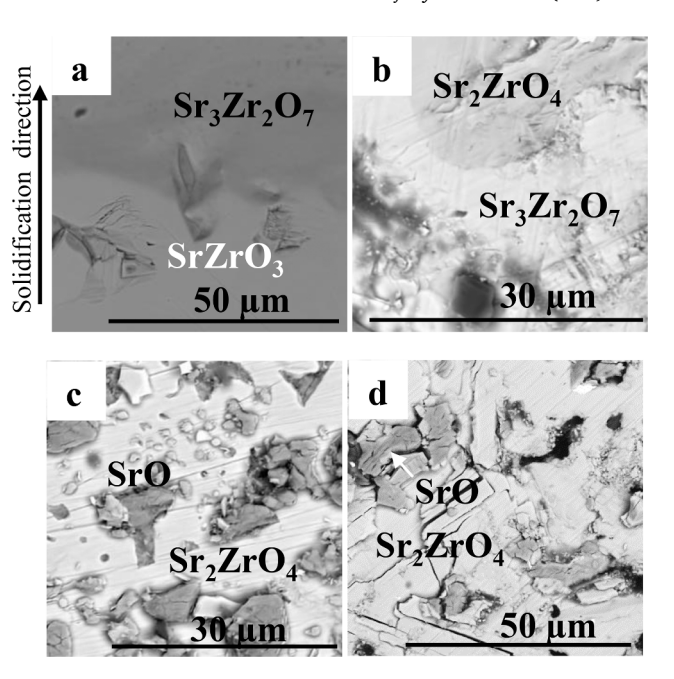


**Fig. 1.** Cross-sectional SEM images of samples solidified using the feeds of (a) 60 mol% SrO, (b) 70 mol% SrO, (c) 75 mol% SrO and (d) 80 mol% SrO.

and lower shafts were melted to form a molten zone in an argon atmosphere with counter rotation at 20 rpm. The molten zone was then separated into two parts at a speed of 5 mm/h by decreasing the lamp power. When using a SrO-excess feed, the disc of the feed was sandwiched between SrZrO<sub>3</sub> sintered rods mounted on the lower and upper shafts, and then the melt-solidification experiments were performed according to the same SCFZ process described above. Since the melting point of SrZrO<sub>3</sub> is about 500 °C higher than that of Sr<sub>3</sub>Zr<sub>2</sub>O<sub>7</sub>, the SrZrO<sub>3</sub> sintered rods were used to hold the molten zone during the meltsolidification experiments, resulting in complete melting of the feed with no contamination from impurities. The solidified samples were cut parallel to the solidified direction and mirror-polished. The texture and composition of the samples were characterized by scanning electron microscopy with energy-dispersive X-ray spectroscopy (SEM/EDS; Hitachi High-Tech, model TM3030 with Min-SVE2107). The phase relation between solid phases and melt was determined on the basis of the textures and compositions of the precipitated phases.

For crystal growth, we utilized the TSFZ method using a solvent of 70 mol% SrO with reference to the results of the SCFZ experiments. The SrO concentration in the feed composition was varied between 60 and 75 mol%, where 60 mol% SrO corresponds to the stoichiometric composition of  $\rm Sr_3Zr_2O_7$ . Feed rods with excess SrO were used to compensate for the strontium component evaporating considerably from the molten zone during the growth. As for the seed, the sintered polycrystalline rod of  $\rm Sr_3Zr_2O_7$  was used. The solvent was put on the top edge of the seed and melted, and then the molten zone was formed by connecting the feed rod to the molten solvent. After that, TSFZ growth was performed in the atmosphere of Ar or  $\rm O_2$  at the growth rates of 2 and 5 mm/h.

The grown crystals were characterized as follows. The texture and composition of the grown crystals were analyzed by an electron probe microanalysis (EPMA; JEOL Ltd., model JXA-8200) and SEM with EDS. Two-dimensional X-ray diffraction analysis (2D-XRD; Bruker Corporation, model Discover D8 with VANTEC-500) was used to identify the crystalline phases and assign Miller indices to the cleavage plane found in the crystals. The crystallinity of the grown crystals was identified by back-reflection Laue X-ray photography. Domain structure and homogeneity in the grown crystals were examined by polarized optical microscopy. Phase transition in the grown crystals was investigated in air

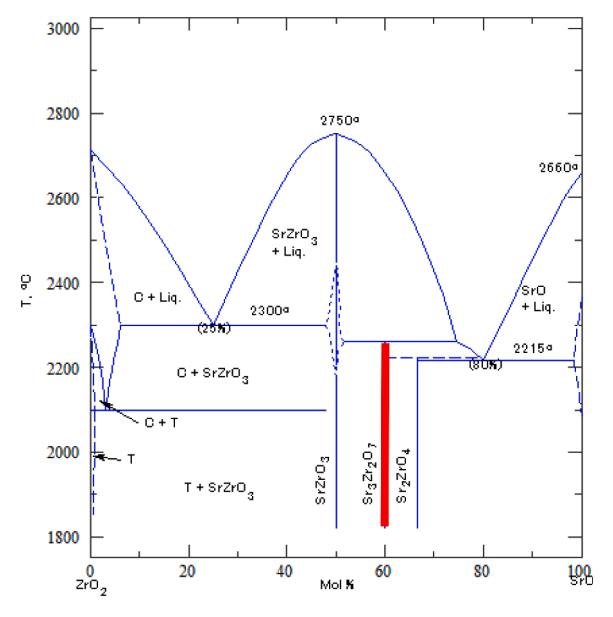


Fig. 2. The phase diagram in the  $ZrO_2$ -SrO system reported by Traverse et al. [16].

by a simultaneous thermogravimetric analyzer with a polarizing microscope (Hitachi High-Tech Science, STA7200RV) at the temperature range between room temperature and 800 °C with the heating and cooling rates of 10 °C/min. Optical SHG measurements were performed in reflection geometry at the temperature range between room temperature and 500 °C using a modified WITec alpha 300S confocal Raman microscope and a LINKAM stage. A pulsed fundamental beam generated by Ti: Sapphire system ( $\lambda=800$  nm, repetition rate of 80 MHz, chopped at 1 kHz) was focused on the sample using a microscope objective.

### 3. Results and discussion

# 3.1. Confirmation of phase diagram in the $ZrO_2$ -SrO system by the SCFZ method

Melting-solidification experiments by the SCFZ method were performed for the samples with varied SrO compositions. Fig. 1 shows cross-section SEM images of the solidified samples. Some solid phases were observed obviously, although the texture was not a typical zonal structure observed for samples obtained by the SCFZ method.

For the stoichiometric composition (Sr<sub>3</sub>Zr<sub>2</sub>O<sub>7</sub>) of 60 mol% SrO,

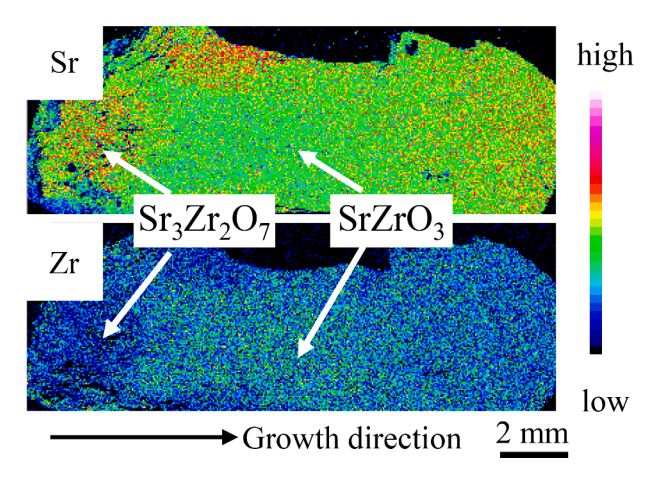


Fig. 3. X-ray intensity distributions of Sr K $\alpha$  and Zr K $\alpha$  in the longitudinal section of the crystal grown by the TSFZ method using  $Sr_3Zr_2O_7$  stoichiometric feed (Run 1).

SrZrO<sub>3</sub> phase precipitated as a primary phase, and then Sr<sub>3</sub>Zr<sub>2</sub>O<sub>7</sub> phase precipitated as shown in Fig. 1a. This result indicates that Sr<sub>3</sub>Zr<sub>2</sub>O<sub>7</sub> melts incongruently to SrZrO3 and a liquid phase, supporting the phase diagram reported by Traverse et al. and Yokokawa et al. [17-18]. For 70 mol% SrO composition, the target Sr<sub>3</sub>Zr<sub>2</sub>O<sub>7</sub> phase precipitated as a primary phase, and then Sr<sub>2</sub>ZrO<sub>4</sub> phase precipitated as seen in Fig. 1b. No precipitation of Sr<sub>4</sub>Zr<sub>3</sub>O<sub>10</sub> phase was observed, which is also consistent with the phase diagram reported by Traverse et al. This result reveals that Sr<sub>3</sub>Zr<sub>2</sub>O<sub>7</sub> phase coexists with the liquid phase near 70 mol% SrO composition. As for 75 and 80 mol% SrO compositions, Sr<sub>2</sub>ZrO<sub>4</sub> phase precipitated as a primary phase, and SrO phase was included in the Sr<sub>2</sub>ZrO<sub>4</sub> phase as shown in Fig. 1c and 1d. These results suggest that Sr<sub>2</sub>ZrO<sub>4</sub> phase is in equilibrium with the liquid phase with a composition close to 75 mol% of SrO, ruling out the possibility of Sr<sub>3</sub>Zr<sub>2</sub>O<sub>7</sub> phase being precipitated from the melt of 75 mol% SrO or more. Therefore, we anticipate that single crystals of Sr<sub>3</sub>Zr<sub>2</sub>O<sub>7</sub> can be obtained by solution growth using SrO-rich solution, for example, self-flux and TSFZ methods using a solvent of about 70 mol% SrO.

The results of the melt-solidification experiments demonstrated that SrZrO<sub>3</sub>, Sr<sub>3</sub>Zr<sub>2</sub>O<sub>7</sub>, Sr<sub>2</sub>ZrO<sub>4</sub>, and SrO phases precipitate from the liquid phase of 60 mol% SrO or more. Of the four compounds, Sr<sub>3</sub>Zr<sub>2</sub>O<sub>7</sub> and Sr<sub>2</sub>ZrO<sub>4</sub> melt incongruently. These facts suggest that the phase diagram reported by Traverse *et al.* shown in Fig. 2 is the most reliable of the previously known phase diagrams [15–18]. According to Traverse's report, the peritectic temperature of the Sr<sub>3</sub>Zr<sub>2</sub>O<sub>7</sub> phase is quite high,

Table 1	
Growth conditions and as-grown crystals.	

Run No.	Atmos-phere	Feed comp. [mol% SrO]	Solvent [mol% SrO]	Growth rate [mm/h]	As-grown crystal
1	Ar	60 (Sr <sub>3</sub> Zr <sub>2</sub> O <sub>7</sub> )	70	5	
2	Ar	66	70	5	
3	Ar	68	70	5	
4	Ar	75	-	5	
5	$O_2$	66	70	5	
6	$O_2$	66	70	2	

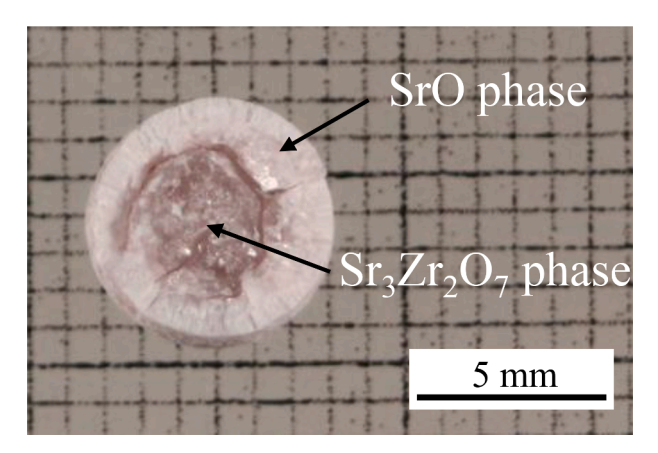


**Fig. 4.** Photograph of the cross-section of crystal (vertical to the growth direction) grown by the TSFZ method using 8 mol% SrO excess feed (Run 3).

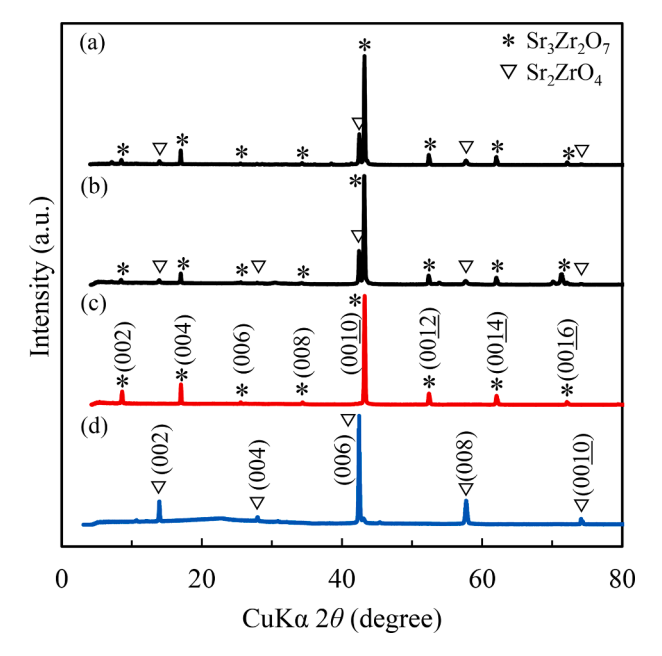


Fig. 5. X-ray diffraction patterns of cleavage planes of crystals grown by various growth conditions shown in Table 1. (a) 68 mol% in Ar (Run 3), (b) 66 mol% in  $O_2$  (Run 5), (c) 66 mol% in  $O_2$  at 2 mm/h (Run 6), (d) 75 mol% in Ar (Run 4).

about 2250 °C, and the eutectic temperature of  $Sr_2ZrO_4$  and SrO is 2215 °C. In addition, the temperature and composition ranges where  $Sr_3Zr_2O_7$  phase coexists with a liquid phase are narrow: 40 °C and about 5 mol% SrO, respectively. Due to the above reasons, the growth of  $Sr_3Zr_2O_7$  single crystals seems to be very challenging.

### 3.2. Crystal growth of Sr<sub>3</sub>Zr<sub>2</sub>O<sub>7</sub> by the TSFZ method

Based on the results of the SCFZ experiment, we attempted to grow single crystals of  $\rm Sr_3Zr_2O_7$  by the TSFZ method using the solvent of 70 mol% SrO composition. The TSFZ growth was carried out under various growth conditions summarized in Table 1. Details of each growth process are described below.

For TSFZ growth using stoichiometric composition feed (Run 1 in Table 1), SrO phase evaporated from the molten zone during growth, and it was difficult to maintain the molten zone throughout the growth process. The EPMA results in Fig. 3 show the spatial distributions of Sr and Zr along the grown direction in the longitudinal cross section. The precipitation of  $Sr_3Zr_2O_7$  phase was detected in regions formed at the

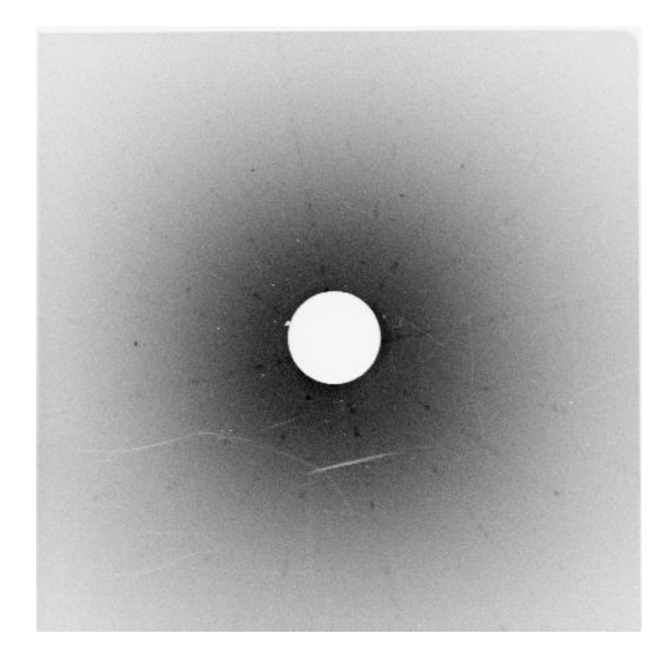


Fig. 6. Back-reflection Laue photograph of  $Sr_3Zr_2O_7$  crystals containing  $Sr_2ZrO_4$  phase grown using 68 mol% SrO feed in Ar atmosphere at 5 mm/h rate.

initial stage of the growth, suggesting that the solvent of 70 mol% SrO is effective in the crystal growth of  $\rm Sr_3Zr_2O_7$ . As crystal growth proceeded, however, the  $\rm SrZrO_3$  phase precipitated as is evident from Fig. 3. This is probably because of a decrease in SrO concentration in the melt caused by its vaporization during crystal growth. From this result, we concluded that charging an excess amount of SrO into the feeds is necessary so that the evaporation of SrO during the crystal growth will be compensated. [23–24].

The results of the crystal growth using feeds with excess SrO are described below. The Sr concentration in the feed was increased to 6 and 8 mol% SrO excess from the stoichiometric composition of 60 mol% SrO; the growth processes are denoted as Runs 2 and 3, respectively. For 6 mol% SrO excess feed (Run 2), the molten zone was unstable and SrZrO<sub>3</sub> phase mainly precipitated in the grown crystals. The situation is similar to that of Run 1 where SrO evaporated extensively. In the case of 8 mol% SrO excess feed (Run 3), on the contrary, the molten zone and lamp output could be kept stable for a longer time. Eventually, Run 3 with 8 mol% SrO excess feed resulted in a grown crystal with a length of 32 mm. SrO, which had evaporated from the molten zone during the crystal growth, was deposited on the surface of the grown crystal. Although the grown crystal looked polycrystalline, colorless and transparent crystals were discovered in the central part as shown in Fig. 4. The obtained crystals are thin flakes with a maximum size of 2 mm square, implying their strong cleavage properties. 2D-XRD data collected for the plate-like crystals display the 00 l peaks of the Sr<sub>3</sub>Zr<sub>2</sub>O<sub>7</sub> structure (see Fig. 5a). The appearance of 00 l diffraction peaks indicates that the ab-plane is welldeveloped. As shown in Fig. 6, the single-crystal nature of the platelike crystals was also confirmed by the back-reflection Laue X-ray photograph. However, a combination of XRD, SEM, and optical microscopy revealed that the plate-like crystals contain needle-like crystals of the Sr<sub>2</sub>ZrO<sub>4</sub> phase. The emergence of Sr<sub>2</sub>ZrO<sub>4</sub> phase in the Sr<sub>3</sub>Zr<sub>2</sub>O<sub>7</sub> matrix is considered due to fluctuation of SrO concentration in the molten zone caused by the supply of SrO from SrO-excess feed and also due to vaporization of SrO from the molten zone. We also grew crystals using the 15 mol% SrO excess feed (75 mol% SrO), which is near the peritectic composition of Sr<sub>3</sub>Zr<sub>2</sub>O<sub>7</sub> (see Run 4 in Table 1). The as-grown crystal had a polycrystalline-like shape as shown in Table 1, but some cleaved crystals up to about 1 mm square were obtained from the sample. They were confirmed to be single crystals of Sr<sub>2</sub>ZrO<sub>4</sub> by the 2D-XRD pattern displayed in Fig. 5d. This result indicates that Sr<sub>2</sub>ZrO<sub>4</sub>

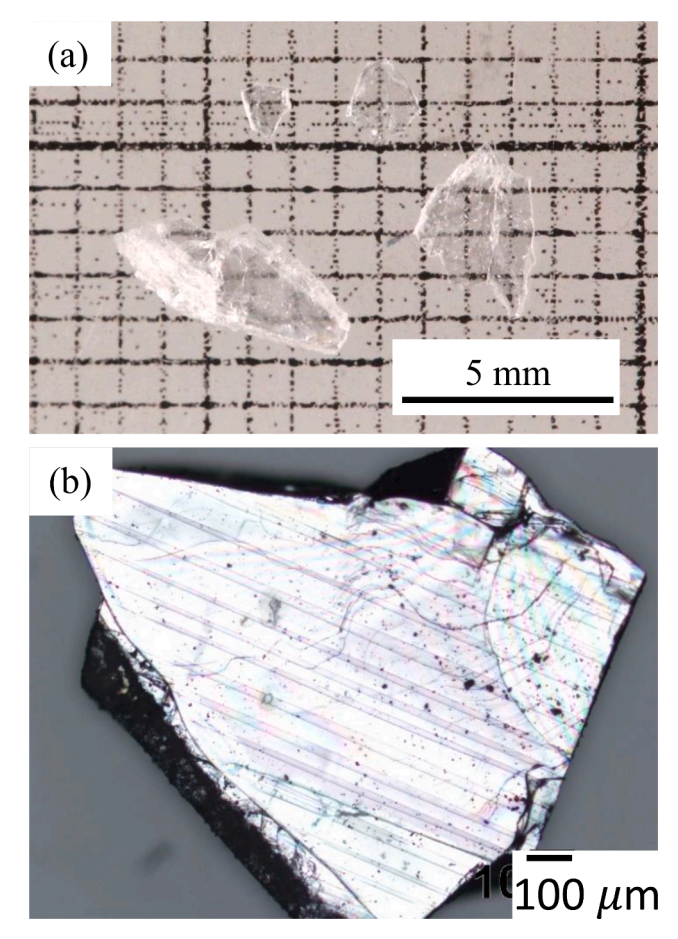


Fig. 7. Single crystals of  $\rm Sr_3Zr_2O_7$  grown under optimized growth conditions. (a) Stereo microphotograph of the overall and (b) Polarized microphotographs of domain structure in the cleaved plane.

phase easily precipitates from the melt when the SrO concentration in the feed is more than the stoichiometric composition of  $\rm Sr_2ZrO_4(66.7~mol\%~SrO)$ . Therefore, it was determined that the use of 6 mol% SrO excess feed (66 mol% SrO) is optimal for the crystal growth of  $\rm Sr_3Zr_2O_7$ . Using such a feed, however, the growth is difficult because of the unstable melting zone and SrO evaporation as exemplified by Run 2.

We next performed crystal growths (Runs 5 and 6 in Table 1) under oxygen instead of an Ar atmosphere with the optimal 6 mol% SrO excess feed. This is because the presence of O<sub>2</sub> would be effective in stabilizing the molten zone as well as suppressing the SrO evaporation. As expected, the molten zones and lamp outputs at Runs 5 and 6 were stable for a long time as compared with Run 2 under an Ar atmosphere. For growth at 5 mm/h (Run 5), however, some cleaved crystal pieces obtained from the as-grown crystals still contained Sr<sub>2</sub>ZrO<sub>4</sub> phase as shown in Fig. 5b. When the growth rate was decreased from 5 to 2 mm/h, an as-grown crystal of 6 mm in diameter and 23 mm long was obtained (see Run 6 in Table 1), from which colorless and transparent crystals were found. Fig. 7(a) illustrates a polarizing microscope image of the crystals, having a typical size of several millimeters and being highly cleavable. We confirmed by the 2D-XRD (Fig. 5c) that the crystals were composed only of Sr<sub>3</sub>Zr<sub>2</sub>O<sub>7</sub> without any secondary phases and that the planes of easy cleavage are perpendicular to the c axis, i.e., (001) planes. Moreover, the composition of the crystals was determined to be stoichiometric by qualitative analysis using EDS. We have successfully grown sizable single crystals of Sr<sub>3</sub>Zr<sub>2</sub>O<sub>7</sub> by finely tuning the growth conditions such as the feed and solvent compositions, growth atmosphere, and growth rate.

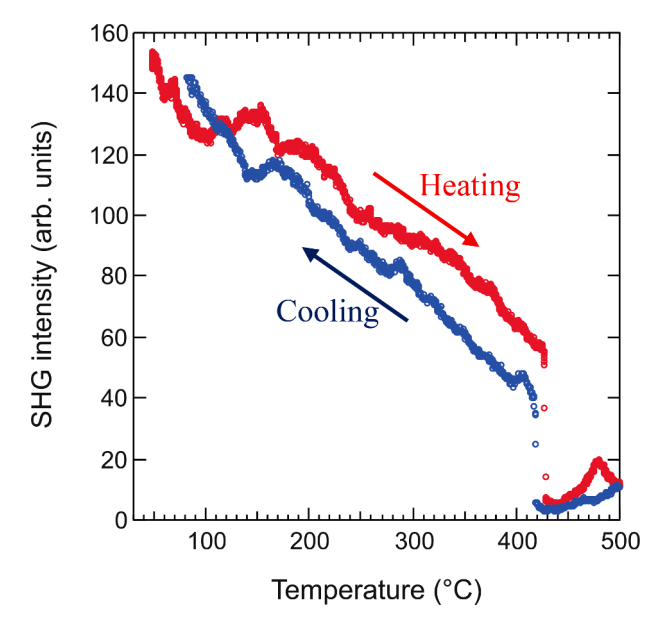
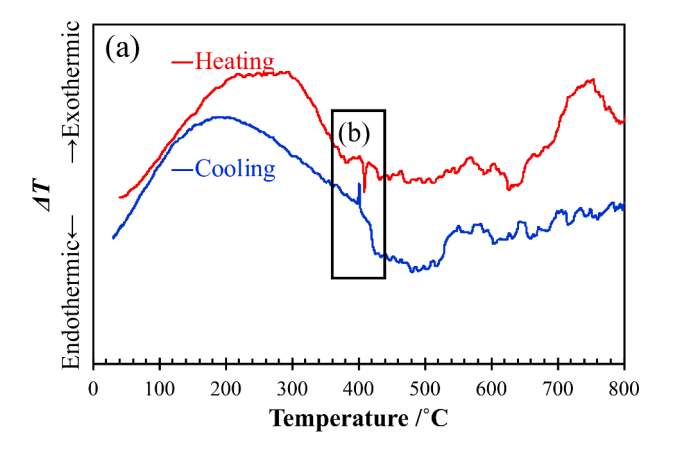


Fig. 8. Temperature dependence of SHG intensity for  ${\rm Sr_3Zr_2O_7}$  single crystal on heating and cooling.



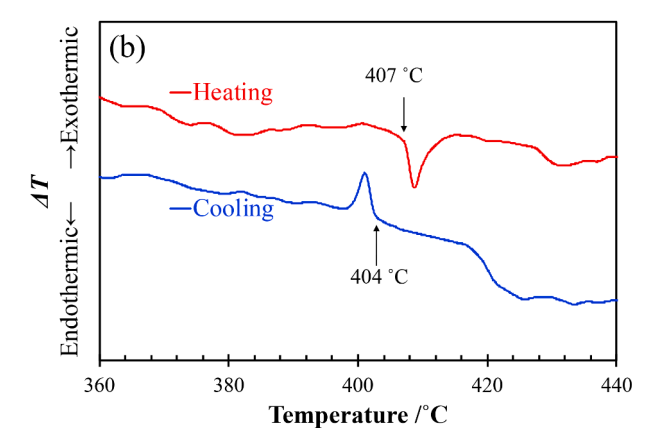


Fig. 9. DTA curves of  $Sr_3Zr_2O_7$  single crystal on heating and cooling between room temperature and 800 °C (a), and between 360 °C and 440°C (b).

# 3.3. Observation of phase transition and domain structure in $Sr_3Zr_2O_7$ crystals

As shown in Fig. 7b, twin domains were clearly seen in the cleaved (001) plane of the Sr<sub>3</sub>Zr<sub>2</sub>O<sub>7</sub> single crystals. HIF-related materials like

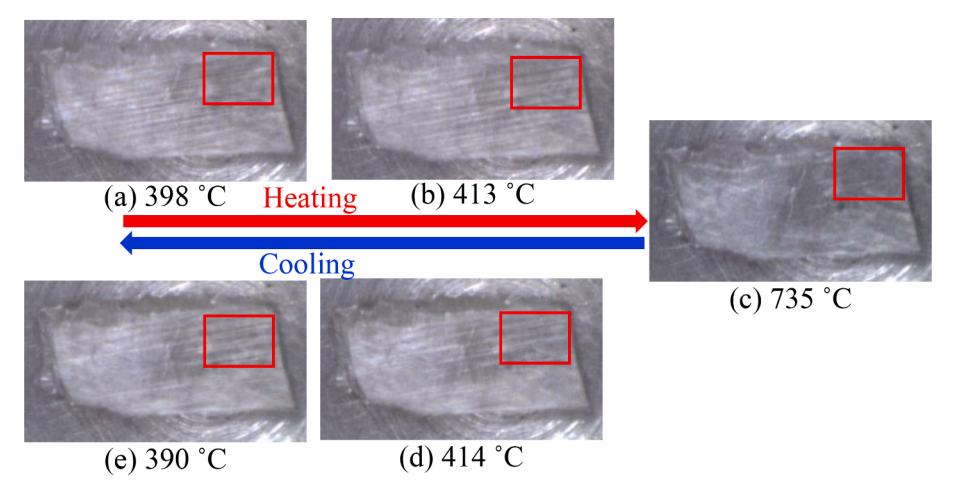


Fig. 10. Polarized microphotographs of Sr<sub>3</sub>Zr<sub>2</sub>O<sub>7</sub> single crystal on heating and cooling.

single-crystal (Ca, Sr)<sub>3</sub>Ti<sub>2</sub>O<sub>7</sub> grown by the FZ method also exhibit such orthorhombic twin boundaries, which are also called ferroelastic domain walls [10]. According to the previous report [14], Sr<sub>3</sub>Zr<sub>2</sub>O<sub>7</sub> adopts four polymorphs depending on the temperature: HIF A21am phase at 27-447 °C, paraelectric Pnab phase at 367-627 °C, Amam phase at 627-767 °C, and I4/mmm phase above 767 °C. Here, the ferroelectric phase transition in Sr<sub>3</sub>Zr<sub>2</sub>O<sub>7</sub> single crystal was investigated by SHG measurements. Fig. 8 shows that the SHG intensity recorded from a Sr<sub>3</sub>Zr<sub>2</sub>O<sub>7</sub> single crystal gradually decreased with increasing temperature and steeply dropped to zero at about 430 °C on heating. This result is consistent with those reported for polycrystalline Sr<sub>3</sub>Zr<sub>2</sub>O<sub>7</sub>, indicating that the HIF A2<sub>1</sub>am phase transforms into a centrosymmetric phase at about 430  $^{\circ}$ C. On cooling, on the other hand, a finite SHG signal appeared at about 420 °C, a slightly lower temperature than the transition temperature on heating. The thermal hysteresis behavior can be explained by the first-order nature of the ferroelectric transition, which has already been demonstrated for the polycrystalline sample [14]. We also examined the relationship between the domain structure and the phase transition in Sr<sub>3</sub>Zr<sub>2</sub>O<sub>7</sub> single crystals utilizing DTA with a polarizing optical microscope. Fig. 9 (a) and (b) show DTA curves recorded for a Sr<sub>3</sub>Zr<sub>2</sub>O<sub>7</sub> single crystal on heating and cooling. A clear endothermic (exothermic) peak was observed on heating (cooling) at 407 (404) °C that can be assigned to the ferroelectric transition identified by the SHG measurements. The thermal hysteresis and the finite latent heat further corroborate the first-order nature of this phase transition. No other phase transitions were apparent from the ferroelectric phase transition temperature up to 800 °C. Fig. 10 shows polarized microphotographs excerpted from the movie available as Supporting Information. We observed that the colors of neighboring domains instantly switched like blind shutters at about 407  $^{\circ}\text{C}$  and the switching was reversible upon heating and cooling. The thermal evolution of the domain structure is due to the phase transition between the ferroelectric A21am and paraelectric Pnab phases. The twin domains still remained above the ferroelectric transition temperature and disappeared completely above about 735 °C accompanied by the phase transition between the orthorhombic *Amam* and tetragonal *I4/mmm* phases. The phase transition between the Pnab and Amam phases, which is expected to occur at around 640 °C [14], was not detectable by direct observation with a polarizing microscope as well as by the DTA results. The Pnab-to-Amam phase transition only involves the disappearance of the ZrO<sub>6</sub> octahedral rotation and keeps the ZrO<sub>6</sub> octahedral tilt unchanged. The twin domains can be created solely by the octahedral tilting, and the loss of the octahedral rotation vanishes merely structural domains within each orthorhombic twin [25]. The resolution of our observation was probably not enough to visualize such a small domain structure and its evolution.

#### 4. Conclusion

The layered perovskite oxide  $Sr_3Zr_2O_7$  with the Ruddlesden-Popper structure is very interesting since it is a novel hybrid improper ferroelectric material whose ferroelectricity is caused by the combination of rotation and tilt of  $ZrO_6$  octahedra. By referring to the melting behavior of  $Sr_3Zr_2O_7$ , we demonstrated the successful growth of its single crystals for the first time by the TSFZ method. The grown crystals are plate-like with a typical size of several millimeters square. Furthermore, we confirmed the ferroelectric phase transition of single crystal  $Sr_3Zr_2O_7$  by temperature-dependent SHG measurements and thermal analysis as well as by direct observation of the domain structures. We anticipate that  $Sr_3Zr_2O_7$  single crystals will pave the way to further studies including the precise characterization of the domain structures and properties and polarized Raman scattering measurements shedding light on the unusual lattice dynamics across the ferroelectric transition.

## CRediT authorship contribution statement

Ikuya Fukasawa: Validation, Formal analysis, Investigation, Writing – original draft. Yuki Maruyama: Resources, Writing – review & editing, Supervision. Suguru Yoshida: Investigation, Writing – review & editing. Koji Fujita: Writing – review & editing, Supervision, Funding acquisition. Hidehiro Takahashi: Resources, Formal analysis. Masataka Ohgaki: Resources, Formal analysis. Masanori Nagao: Resources, Supervision. Satoshi Watauchi: Resources, Supervision. Venkatraman Gopalan: Supervision. Katsuhisa Tanaka: Writing – review & editing, Supervision, Funding acquisition. Isao Tanaka: Writing – review & editing, Project administration, Funding acquisition.

## **Declaration of Competing Interest**

The authors declare that they have no known competing financial interests or personal relationships that could have appeared to influence the work reported in this paper.

### Data availability

No data was used for the research described in the article.

### Acknowledgment

This work was partly financially supported by JSPS KAKENHI grant numbers JP20K20546, JP21H04619, and JP22H01775. The SHG work at Penn State was supported by the National Science Foundation (Grant No. DMR-2210933). K. F. acknowledges grants from the Murata Science

Foundation, the lketani Science and Technology Foundation, the Nippon Sheet Glass Foundation for Materials Science and Engineering, the Mitsubishi Foundation, the Okura Kazuchika. Memorial Foundation, and Izumi Science and Technology Foundation.

### Appendix A. Supplementary material

Movie of domain structure observation with DTA curve on heating and cooling (MP4).

Supplementary data to this article can be found online at https://doi.org/10.1016/j.jcrysgro.2023.127241.

#### References

- [1] M. Kohli, C. Wuethrich, K. Brooks, B. Willing, M. Forster, P. Muralt, N. Setter, P. Ryser, Pyroelectric thin-film sensor array, Sens. Actuators, A 60 (1997) 147–153.
- [2] C.B. Eom, S.T. McKinstry, Thin-film piezoelectric MEMS, MRS Bull. 37 (2012) 1007–1017.
- [3] H. Kueppers, T. Leuerer, U. Schnakenberg, W. Mokwa, M. Hoffmann, T. Schneller, U. Boettger, R. Waser, PZT thin films for piezoelectric microactuator applications. Sens. Actuators, A 97-98 (2002) 680-684.
- [4] J.K. Burdett, Use of the Jahn-Teller theorem in inorganic chemistry, Inorg. Chem. 20 (1981) 1959–1962.
- [5] S.N. Ruddlesden, P. Popper, New compounds of the K<sub>2</sub>NiF<sub>4</sub> type, Acta Crystallogr. 10 (1957) 538–539.
- [6] N.A. Benedek, C.J. Fennie, Hybrid Improper Ferroelectricity: A Mechanism for Controllable Polarization-Magnetization Coupling, Phys. Rev. Lett. 106 (2011), 107204.
- [7] N.A. Benedek, A.T. Mulder, C.J. Fennie, Polar octahedral rotations: A path to new multifunctional materials, J. Solid State Chem. 195 (2012) 11–20.
- [8] N.A. Benedek, J.M. Rondinelli, H. Djani, P. Ghosez, P. Lightfoot, Understanding ferroelectricity in layered perovskites: new ideas and insights from theory and experiments, Dalt. Trans. 44 (2015) 10543–10558.
- [9] A.B. Harris, Symmetry analysis for the Ruddlesden-Popper systems  $Ca_3Mn_2O_7$  and  $Ca_3Ti_2O_7$ , Phys. Rev. B 84 (2011), 064116.
- [10] Y.S. Oh, X. Luo, F.T. Huang, Y. Wang, S.W. Cheong, Experimental demonstration of hybrid improper ferroelectricity and the presence of abundant charged walls in (Ca, Sr<sub>3</sub>3T<sub>i</sub>2<sub>0</sub>7 crystals, Nat. Mater. 14 (2015) 407–413.

- [11] M.S. Senn, A. Bombardi, C.A. Murray, C. Vecchini, A. Scherillo, X. Luo, S. W. Cheong, Negative Thermal Expansion in Hybrid Improper Ferroelectric Ruddlesden-Popper Perovskites by Symmetry Trapping, Phys. Rev. Lett. 114 (2015), 035701.
- [12] X.Q. Liu, J.W. Wu, X.X. Shi, H.J. Zhao, H.Y. Zhou, R.H. Qiu, W.Q. Zhang, X. M. Chen, Hybrid improper ferroelectricity in Ruddlesden-Popper Ca<sub>3</sub>(Ti, Mn<sub>)</sub>2<sub>0</sub>7 ceramics, Appl. Phys. Lett. 106 (2015), 202903.
- [13] S. Yoshida, H. Akamatsu, R. Tsuji, O. Hernandez, H. Padmanabhan, A.S. Gupta, A. S. Gibbs, K. Mibu, S. Murai, J.M. Rondinelli, V. Gopalan, K. Tanaka, K. Fujita, Hybrid Improper Ferroelectricity in (Sr. Ca) $^{3}$ Sn $^{2}$ O7 and Beyond: Universal Relationship between Ferroelectric Transition Temperature and Tolerance Factor in n=2 Ruddlesden-Popper Phases, J. Am. Chem. Soc. 140 (2018) 15690–156700.
- [14] S. Yoshida, K. Fujita, H. Akamatsu, O. Hernandez, A.S. Gupta, F.G. Brown, H. Padmanabhan, A.S. Gibbs, T. Kuge, R. Tsuji, S. Murai, J.M. Rondinelli, V. Gopalan, K. Tanaka, Ferroelectric Sr3Zr2O7: Competition between Hybrid Improper Ferroelectric and Antiferroelectric Mechanisms, Adv. Funct. Mater. 28 (2018) 1801856.
- [15] G. Tilloca, M. Perez, Y. Jorba, X-ray characterization of  $Sr_3Zr_2O_7$  hydrate, Rev. Hautes Temp. Refract. 1 (1964) 331–342.
- [16] T. Noguchi, T. Okubo, O. Yonemochi, Reactions in the System ZrO<sub>2</sub>-SrO, J. Am. Ceram. Soc. 52 (1969) 178–181.
- [17] J.P. Traverse, M. Foex, Études des systèmes formés par la zircone avec la chaux et l'oxyde de strontium, High Temp. –High Pressures 1 (1969) 409–427.
- [18] H. Yokokawa, N. Sakai, T. Kawada, M. Dokiya, Phase diagram calculations for ZrO<sub>2</sub> based ceramics: thermodynamic regularities in zirconate formation and solubilities of transition metal oxides, Sci. Technol. Zirconia V 16 (1992) 59–68.
- [19] S. Kimura, I. Shindo, Single crystal growth of YIG by the floating zone method, J. Cryst. Growth 41 (1977) 192–198.
- [20] I. Tanaka, H. Kojima, Superconducting Single-Crystals, Nature 337 (1989) 21-22.
- [21] I. Shindo, Determination of the phase diagram by the slow cooling float zone method: The system MgO-TiO<sub>2</sub>, J. Cryst. Growth 50 (1980) 839–851.
- [22] I. Tanaka, R. Yoshihara, C. Nakazawa, M. Nagao, S. Watauchi, Determination of the phase relation of a Li<sub>x</sub>La<sub>(1-x)/3</sub>NbO<sub>3</sub> system by the slow cooling floating zone method, J. Cryst. Growth 507 (2019) 251–254.
- [23] D. Souptel, G. Behr, A.M. Balbashov, SrZrO<sub>3</sub> single crystal growth by floating zone technique with radiation heating, J. Cryst. Growth 236 (2002) 583–1568.
- [24] S.I. Ikeda, U. Azuma, N. Shirakawa, Y. Nishihara, Y. Maeno, Bulk single-crystal growth of strontium ruthenates by a floating-zone method, J. Cryst. Growth 237–239 (2002) 787–791.
- [25] E.A. Nowadnick, C.J. Fennie, Domains and ferroelectric switching pathways in Ca<sub>3</sub>Ti<sub>2</sub>O<sub>7</sub> from first principles, Phys. Rev. B 94 (2016), 104105.